Journal of Materials Chemistry C

COMMUNICATION

View Article Online
View Journal | View Issue

Published on 05 October 2016. Downloaded by Incheon National University on 18/11/2016 05:18:55.

Cite this: J. Mater. Chem. C, 2016, 4, 9947

Received 3rd August 2016,
Accepted 5th October 2016

DOI: 10.1039/c6tc03329f

www.rsc.org/MaterialsC

Transparent ITO mechanical crack-based pressure and strain sensor†

Taemin Lee,‡[ab] Yong Whan Choi,‡[a] Gunhee Lee,[ab] Peter V. Pikhitsa,[a] Daeshik Kang,[c] Sang Moon Kim[d] and Mansoo Choi*[ab]

Sensors to detect motion with high precision have been extensively studied in diverse engineering research fields. Among them, transparent devices, which have strong adaptability in various fields such as display panels, have not gained much academic interest. In this study, we present a highly sensitive pressure and strain sensor based on a cracked transparent epilayer, indium-tin oxide (ITO), deposited on a transparent PET substrate. This sensor system, with which we demonstrate how to detect pressure and finger motions, exhibits ultra-sensitivity to strain (gauge factor about 4000 at 2% strain), pressure (sensitivity is about 1.91 kPa^{-1} at pressures from 30 to 70 kPa), and transparency (up to 89% at a wavelength of 560 nm). Also, durability has been validated over 5000 cycles. The sensor thus boasts broad applications including touchscreens and motion detectors.

1. Introduction

Complying with human needs of electronic devices is an essential component of future device applications.[1–8] In order to adapt electronic devices to the human body, various studies have been conducted.[4,5,9–13] The existing sensors, however, are opaque due to the property of the materials they use.[1,14–16] These include a recently reported mechanical crack sensor, which has high sensitivity, determined as a linearly defined gauge factor (GF, expressed through the normalized resistance R/R_0 variation with the strain ε: $(R/R_0)/\varepsilon > 2000$) and high flexibility, but which is also opaque as it uses platinum.[1] Sensors with opaque surfaces have limitations since various fields require transparent devices with strong adaptability for use in many applications, such as display panels. Several studies on transparent electronics have been reported.[17–26] However, only a few studies have shown transparent strain sensors.[22–25] Among them, are several transparent strain sensors based on carbon nanotubes,[22] silver nanowires,[23,24,26] and graphene,[25,27] which also have both advantages and limitations in terms of transparency or sensitivity. Specifically, even though the sensor reported by Lipomi *et al.*[22] has transparency up to 79%, its pressure sensitivity defined as $(R/R_0)/p$, where p denotes the applied pressure, is 2.3×10^{-4} kPa^{-1} and the strain gauge factor is 0.4. Next, a transparent silver nanowire strain sensor has been reported with transparency up to 75%, but with a low gauge factor ($\leq$12.4).[23] Other researchers have demonstrated a graphene-based transparent strain sensor[25] with good transparency (75–80%), but also with very low sensitivity (GF < 15). As can be seen, producing a sensor with high transparency and sensitivity is quite a challenging job. To tackle this challenge, we present a mechanical crack sensor to measure strain and pressure with the transparent conductor indium tin oxide (ITO). Our transparent crack sensor has high transparency with a clear view up to 89% (at a wavelength of 560 nm), and high sensitivity to strain (GF reaches about 4000 at strain of 2%) and pressure (with sensitivity of about 1.91 kPa^{-1} at pressures of 30–70 kPa). High transparency of the sensor comes from the intrinsic transparency of the materials used (ITO, polyethylene terephthalate (PET)). However, cracks on a transparent film generally distort the image underneath. In order to avoid such distortion from cracks, unlike the previous work, which used a polyurethane acrylate (PUA) over PET,[1] we used only the PET substrate since PET film deposited with ITO is widely used in transparent electrodes.[18,28,29] The problem when using PUA is that it is cracked along with the epilayer, which generates deep and broad cracks of widths comparable to visible light wavelengths. With the PET substrate used in this study, we obtained insensitivity of the underlying visible image to the existence of

[a] Global Frontier Center for Multiscale Energy Systems, Department of Mechanical and Aerospace Engineering, Seoul National University, Seoul 151-742, Korea. E-mail: mchoi@snu.ac.kr
[b] Division of WCU Multiscale Mechanical Design, Department of Mechanical and Aerospace Engineering, Seoul National University, Seoul 151-742, Korea
[c] Department of Mechanical Engineering, Ajou University, San 5, Woncheon-dong, Yeongtong-gu, Suwon 443-749, Republic of Korea
[d] Department of Mechanical Engineering, Incheon National University, Incheon, 406-772, Korea

† Electronic supplementary information (ESI) available. See DOI: 10.1039/c6tc03329f

‡ These authors contributed equally to this work.

Published on 05 October 2016. Downloaded by Incheon National University on 18/11/2016 05:18:55.

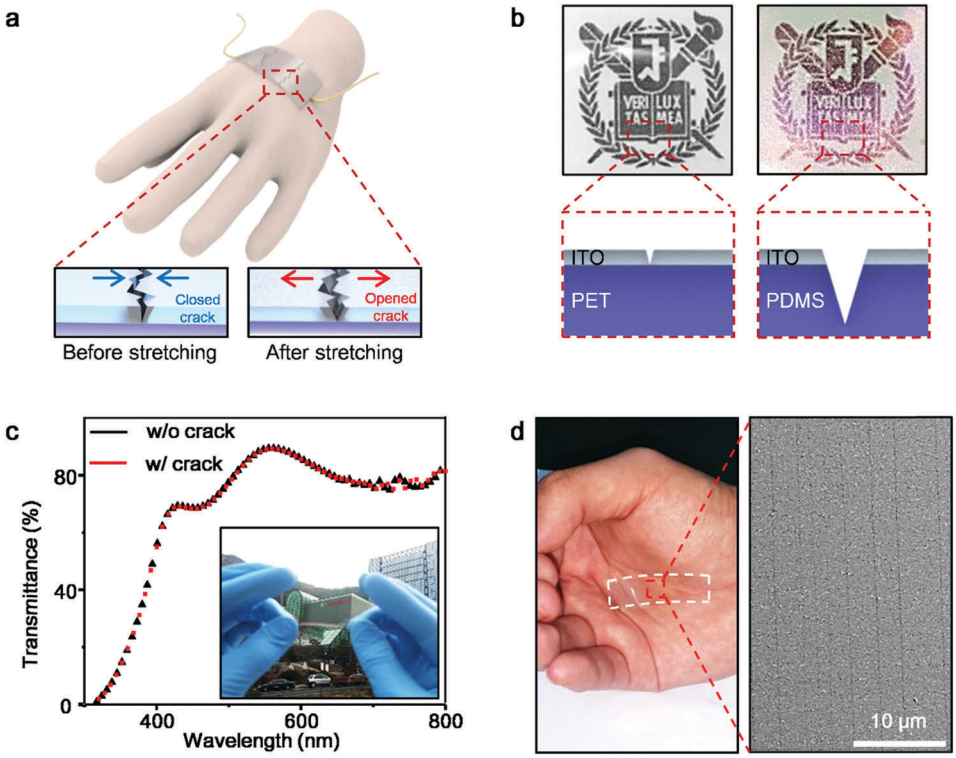

Fig. 1 Schematic descriptions and images of a transparent crack sensor. (a) The image of a transparent crack sensor on a human hand with illustrations of the sensor cracks less opened (bottom left), and more opened (bottom right). (b) Images on the top shown through the ITO crack sensors on PET film (on the left) and on PDMS film (on the right) with their cross-sectional schematic illustrations below each image. (c) A graph of transmittance *versus* light wavelength through the crack sensor. Red and black dots represent the transmittance of ITO crack sensor with and without cracks, respectively. The inset image presents the transparent ITO crack sensor held up to show the background behind. (d) The ITO crack sensor on a palm (left), and its FESEM image (right) in which the cracks on the sensor are parallel to each other.

cracks on the ITO films because the wavelength of visible light (400–700 nm) is much larger than the gap opening (~100 nm) of a crack and much less than the distance (~14 μm) between the cracks. The high sensitivity comes from the straightness of the crack lips and the dramatic increase in the resistance of the ITO layer during the crack opening.

2. Experimental

2.1 ITO crack sensor fabrication

Indium tin oxide (ITO) is deposited on the 30 μm polyethylene terephthalate (PET) film by a sputter (sputter; Ultech Inc.). Deposition time of ITO on the PET film is 45 minutes, whereas a power of 200 W is applied and its thickness is about 600 nm.[18] Since the glass transition temperature is low, the post-annealing process that requires a high temperature condition has been skipped.[30] Before measuring the resistance change, a crack is generated on the crack sensor by stretching with a materials testing machine (3342 UTM, Instron Co.). Resistance is measured by a LabVIEW-based PXI-4071 system (National Instruments Inc.).

2.2 Multi-pixel array sample fabrication

To measure pressure with extended scale, 16 pixels (4 × 4 pixel array) with a square area of 1 × 1 cm^2 is fabricated. Each pixel functions as a pressure sensor. The transparent sensor pixel matrix is applied to a display panel shown in Fig. 3c. ITO is deposited by the sputter through a shadow mask, which has the 4 × 4 pixel array area opened (Fig. S9a, ESI†). To operate the pressure sensor, it needs space between the display panel and itself to be bent. Fig. S9c (ESI†) demonstrates 16 pixels floated and held by polydimethylsiloxane (PDMS) separately. To concentrate a bending effect on the pixels, the edges of the pixels facing each other were cut.

2.3 Pressure measurement of the crack sensor

To measure the pressure, plastic bricks of 1.2 g and 1.8 g in weight were put on different positions on the multi-pixel array pressure sensor. The continuous pressure was measured by applying pressures ranging from 0 to 70 kPa with a load cell (2712-041, Instron Co.) and LabVIEW-based PXI-4071 resistance analyzer (NI Inc.).

3. Results and discussion

3.1 Transparent mechanical crack-based strain sensor

The illustration in Fig. 1a shows the basic features of the ITO crack sensor, which is transparent, flexible, and can be applied on human skin to sense the slightest motion. The sensor is fabricated with ITO (600 nm thickness) sputtered on the PET

 This journal is © The Royal Society of Chemistry 2016

Published on 05 October 2016. Downloaded by Incheon National University on 18/11/2016 05:18:55.

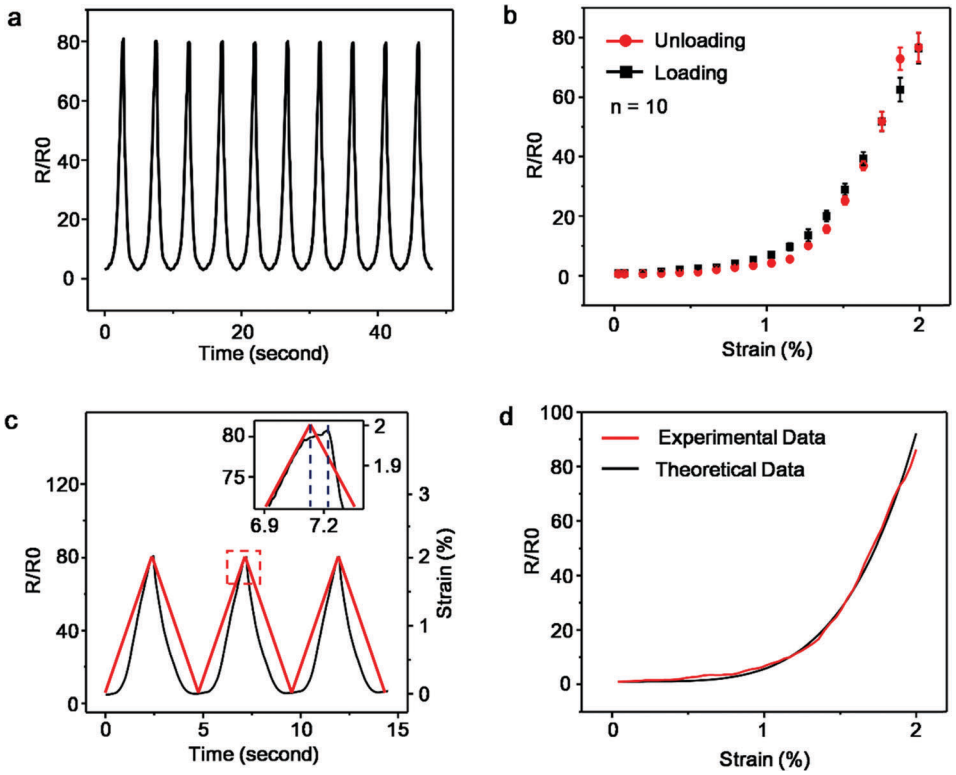

Fig. 2 The variations of the performance of the ITO crack sensor with enhanced strain of 2%. (a) The graph of normalized resistance variance *versus* strain of 2% in a 10-times cyclic test. (b) The standard deviation and the average over 10 different samples in the hysteresis test of the ITO crack sensor. Red and black dots show unloading and loading cases, respectively. (c) The response time of the ITO crack sensor. The red and black lines indicate the input signal (strain of 2%) and the response time of input strain, respectively. The inset graph represents the magnified image of the response time near the peak. (d) Theoretical data of the ITO crack sensor compared to the experimental data.

film (30 μm thickness) after being stretched up to 2% strain to generate cracks on the ITO layer (see details in the Fig. S1, ESI†). The mechanism of the ITO crack sensor is based on the change of the resistance of the ITO layer with the applied strain.[18] Due to the highly non-linear dependence of the resistance *versus* strain (Fig. 2), the sensor responses dramatically to the crack opening. The strained state is characterized by a high local GF. More the strain applied on the sensor, more the cracks are opened (Fig. 1a; bottom right). Therefore, the resistance increases as the opened crack gaps block the conductivity of the ITO film. In contrast, when the cracks are closed (Fig. 1a; bottom left) the resistance decreases. The scanning electron microscopy (SEM) image in Fig. 2Sb (ESI†) shows that the asperity of the crack allows the interconnection through the crack gap at a strain of 2%. Due to the interconnections, some conductivity persists across the crack gaps. In general, cracks on a transparent surface could distort the image underneath. The image at the top right corner of Fig. 1b shows the ITO film deposited on polydimethylsiloxane (PDMS) film. The image at the top left corner is the ITO film deposited on a PET film. Compared to the clearer image on the left, the ITO film on the PDMS film shows a foggy and reddish image of the logo of Seoul National University (SNU), which is placed under the sensor. This distortion occurs because the cracks are generated with enlarged gap widths, not only in the ITO film but also in the PDMS film.[19] The reason for the insensitivity of the transparent ITO sensor on the PET film to the strain of up to 2% is evident from examining its SEM images. The SEM images in Fig. S2 (ESI†) and Fig. 1d on the right show that the crack gap size is below 100 nm, and the distance between each parallel crack is around 14 μm on average. The effect of the cracks on the transmittance of the ITO crack sensor is negligible because the crack gap size (below 100 nm) under a strain of 2% is much smaller than the wavelength of visible light. On the contrary, the sizes of the gap and depth of the ITO crack on PDMS are about 1.8 μm and 1 μm, respectively (Fig. S3, ESI†). Since the thickness of the ITO film is about 600 nm, the crack depth of 1 μm indicates that the cracks are formed not only on the ITO film but also on the PDMS film. However, the ITO crack depth on the PET film is about 600 nm, which is equal to the thickness of the ITO film. The depth and the width of cracks on the PDMS film are much greater and larger, respectively, than on the PET film. The AFM image of the crack on the PDMS film is shown in Fig. S3 (ESI†). The depth of the cracks is strongly related to their width. Fig. 1c presents the transmittance of the ITO crack sensor at different wavelengths. Black triangles and red dots represent the transmittance before and after the crack generation, respectively. Due to the transparency of the ITO sensor, the logo of SNU, which is placed under the sensor can be clearly seen. The average transparency of the ITO crack senor is about 79% in the visible spectrum (with wavelengths from 390 nm to 700 nm).

Published on 05 October 2016. Downloaded by Incheon National University on 18/11/2016 05:18:55.

The left image in Fig. 1d shows how such a highly transparent ITO sensor has enough flexibility to be applied on a human palm.

3.2 Theoretical analysis of the transparent mechanical crack-based strain sensor

Cracks on the ITO-covered PET film are characterized by bridging electrical contacts between crack lips that gradually disconnect while stretching and fewer contact points remain when the sensor is stretched up to 2%. The reverse process should return the sensor to its initial state. To check the reversibility, reproducibility, response time and durability we performed several cycling experiments. Fig. 2a shows a representative set of 10 cycles of strain from 0% to 2%, which are nearly identical. The linearly defined GF $(R/R_0)/\varepsilon$ of the ITO crack sensor would reach over 4000. Fig. 2b is a graph of the normalized resistance *versus* strain curve averaged over ten different samples of ITO crack sensors along with error bars. Black dots for ITO crack sensors are for loading the sensor to the final strain of 2%, and red dots are for unloading. The hysteresis of loading/unloading is small. Fig. S4 (ESI†) is a graph for the loading and unloading test of the ITO crack sensor with variation in strain of 0.5%, 1.0% and 1.5%. Fig. 2c is a magnified part of Fig. 2a and shows the response time (see the inset image in Fig. 2c) of about 1 ms of the ITO crack sensor during the cycling with the stretch speed of 10 mm min^{-1}, which is acceptable for its application. Another important performance is durability, which we tested in a series of more than 6000 cycles. After some adaptation period, the sensor shows good stability at 5000 and onwards cycles (see Fig. S5, ESI† for the marathon test results). The curve of the strain-dependent gauge factor defined as the derivative of resistance normalized to the initial resistance at 0% with respect to the strain of 2% is shown in Fig. S6a (ESI†). Since the curve of the normalized resistance *versus* strain of the ITO crack sensor is super-linear, the strain-dependent gauge factor goes high as the strain increases.

In Fig. 2d, we plot the experimental, normalized resistance *versus* strain along with the theoretical fit that comes from the universal mechanism for a strain sensor based on parallel cracks, which has been reported in a recent work,[1] where a simplified formula was presented as a power law:

$$R/R_0 = 1 + (\varepsilon/\varepsilon_0)^B \quad (1)$$

with fitting parameters $\varepsilon_0 = 0.7$ and $B = 4.7$. In addition, the cycling experiment was performed at a much slower scanning rate of 0.1 mm min^{-1}, which results in similar resistance *versus* strain curves shown in Fig. S7 (ESI†) characterized by $\varepsilon_0 = 0.7$ and $B = 4.1$. A slight difference in parameters comes from the hysteresis phenomenon that usually makes the system rate-sensitive. The good fitting indicates that the ITO crack sensor follows the same mechanism that was already found for a parallel crack sensor based on a Pt film.[1] However, the fitting parameters are quite

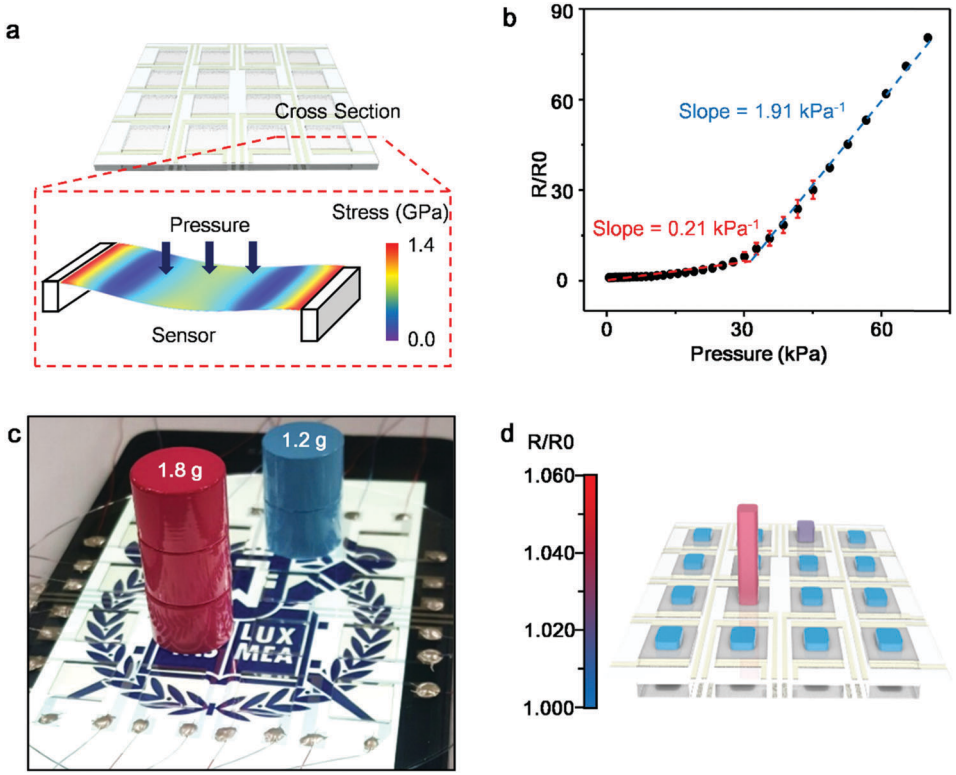

Fig. 3 The transparent pressure sensor and its multi-array based on the ITO crack sensor mechanism. (a) The schematic of the 4 × 4 ITO pressure sensor pixel matrix. The image on the bottom shows the visualized stress data of a single pixel of the pressure sensor. (b) The graph of normalized resistance *versus* pressure ranging from 0 to 70 kPa. The slope of the normalized resistance *versus* pressure from 0 to 30 kPa is 0.21 kPa^{-1}, and from 30 to 70 kPa is 1.91 kPa^{-1}. (c) The image of the transparent pressure sensor multi-array on a display panel. Weights of 1.2 and 1.8 g are put on the different pixels of the multi-array. (d) The normalized resistance change *versus* pressure induced by the weights of 1.2 g and 1.8 g (from (c)).

 This journal is © The Royal Society of Chemistry 2016

Published on 05 October 2016. Downloaded by Incheon National University on 18/11/2016 05:18:55.

varied due to the different characteristics of materials used in Pt/PUA/PET systems.[1] Specifically, as far as ε_0 is defined as the strain, at which the crack gap size coincides with the grain size (the ITO grain here), the difference between the current $\varepsilon_0 = 0.7\%$ and previous $\varepsilon_0 = 0.39\%$ may come from different grain sizes of ITO and Pt and the different proportionality coefficient between the crack gap size *versus* strain (see Kang *et al.*[1]). The other parameter $B = 4.7$ indicates lower asperity of the crack lips compared with the previous $B = 2.3$ found by D. Kang *et al.*[1]

For sensor applications that deal with slight deformations, such as sound vibrations,[1] the local GF is relevant and can be defined from eqn (1)

$$g(\varepsilon) = \mathrm{d}\ln(R)/\mathrm{d}\varepsilon = \frac{B}{\varepsilon_0}\frac{(\varepsilon/\varepsilon_0)^{B-1}}{\left(1+(\varepsilon/\varepsilon_0)^{B}\right)}. \quad (2)$$

Eqn (2) describes the amplification of the sensor response (*e.g.* for vibrations) at a given strain ε. It has a maximum

$$g_{\max} = \frac{(B-1)^{\frac{B-1}{B}}}{\varepsilon_0} \times 100 \quad (3)$$

at the strain (measured in %)

$$\varepsilon_{\max} = (B-1)^{1/B}\varepsilon_0 \quad (4)$$

which makes $g_{\max} = 400$ and $\varepsilon_{\max} = 0.92\%$ (see Fig. S5b, ESI†) against $g_{\max} = 300$ and $\varepsilon_{\max} = 0.43\%$ according to D. Kang *et al.*[1]

3.3 Transparent mechanical crack-based pressure sensor

The transparent ITO crack sensor can act as a pressure sensor. Fig. 3a is the schematic of pressure sensing with the ITO crack film. In the experiment, the edges of the crack sensor are held onto two bars and when the pressure increases, the crack sensor is bent, cracks on the convex ITO surface are opened and the resistance changes. The sensor can distinguish between strain and pressure change depending on the sensor frame structure Fig. S8 (ESI†). We fabricated the ITO crack sensor with a sensing matrix of 4 × 4 pixels (see Fig. S9, ESI†). Each of the ITO pressure sensing pixels has the area of 1 × 1 cm. Each pixel is held by PDMS pillars. Silver was used as a transparent electrode with a thickness of 13 nm. Fig. 3b is a graph of the normalized resistance *versus* pressure varying from 0 to 70 kPa. The slope of the curve of pressure *versus* normalized resistance at pressures from 0 to 30 kPa is about 0.21 kPa^{-1} and it is about 1.91 kPa^{-1} in the range from 30 kPa to 70 kPa. The two slopes in the graph just show a convenient engineering approximation according to the range. Fig. 3c is an image of the ITO pressure sensor pixel matrix lying on a display panel of a mobile phone. The logo of SNU is clearly seen through the

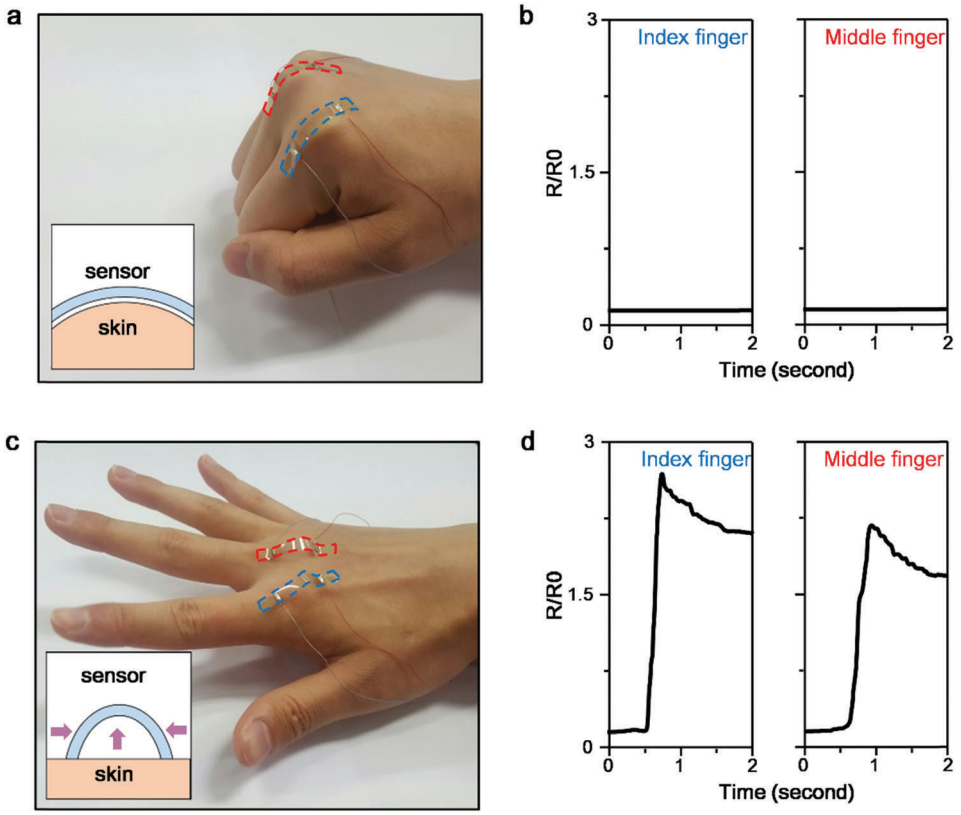

Fig. 4 The normalized resistance variations of the ITO crack sensor induced by fist movement. (a) The ITO crack sensors are attached on the knuckles of the index and the middle fingers of a clenched fist. (b) The graphs represent the normalized resistance variations along with/according to the movements of the index (left plot) and middle (right plot) fingers when the hand is clenched into a fist. (c) When the hand opens, the curvature radius of the ITO crack sensor is diminished. (d) The graphs represent the ITO crack sensor normalized resistance variations due to the movements of the index (left plot) and middle (right plot) fingers when the hand opens.

Published on 05 October 2016. Downloaded by Incheon National University on 18/11/2016 05:18:55.

ITO pressure sensor. Plastic cylinders of 1.8 g and 1.2 g in weight were placed on and pressed the ITO pressure sensor pixels. The resistance change of the pixels induced by the plastic weights is recorded (Fig. S10, ESI†) and it shows that the sensor can measure both the position and the pressure at the same time (Fig. 3d).

3.4 Detecting finger motions with the transparent crack sensor

The ITO crack sensor can detect motion in humans. Since it has sufficient flexibility, the sensor can easily be mounted on a human hand by attaching the ends of the sensor (see Fig. 4a) to measure the strain generated by the motion of the finger. To prove this, one of the experimenters has clenched his fist and had two crack sensors mounted on the knuckles of the index and middle finger, as shown in Fig. 4a. As the radius of curvature of a knuckle is about 3 cm, the surface of the sensor is only slightly stretched, as shown schematically in the inset image of Fig. 4a, which results in no resistance change (Fig. 4b). The human skin under the sensor can be seen and it demonstrates the transparency of the ITO crack sensor. The sensor on the knuckle is slightly folded when the hand opens, as shown in Fig. 4c, to obtain about a 5 mm radius of curvature. The small curvature makes the surface of the sensor stretch and the sensor resistance is increased. The movement of each finger can be measured individually by the resistance change of each of the mounted sensors, as shown in Fig. 4d.

4. Conclusion

In conclusion, we report a transparent pressure and strain crack sensor with high sensitivity based on the parallel crack system in the ITO layer on a polymer substrate. It shows high gauge factors without losing transparency during stretching and can be applied as a multifunctional sensor for detecting strain, pressure and human finger movements. These results indicate that our sensor has considerable performance advantages compared to the flexible and transparent sensors previously introduced.[3,10,17,20,22,23,25] The reproducibility, reversibility, flexibility, durability and large-area coverage through multiplexing enable the application of the device onto curvilinear human skin and in advanced tools.

Acknowledgements

We thank Seong Min Kang for his advice on the experimental methods. This work was supported by the Global Frontier R&D Program in the Center for Multiscale Energy System (NRF-2012M3A6A7054855) funded by the National Research Foundation under the Ministry of Science, ICT & Future, Korea.

References

1 D. Kang, P. V. Pikhitsa, Y. W. Choi, C. Lee, S. S. Shin, L. Piao, B. Park, K. Y. Suh, T. I. Kim and M. Choi, *Nature*, 2014, **516**, 222.
2 D.-H. Kim, N. Lu, R. Ma, Y.-S. Kim, R.-H. Kim, S. Wang, J. Wu, S. M. Won, H. Tao and A. Islam, *Science*, 2011, **333**, 838.
3 S. Lee, A. Reuveny, J. Reeder, S. Lee, H. Jin, Q. Liu, T. Yokota, T. Sekitani, T. Isoyama, Y. Abe, Z. Suo and T. Someya, *Nat. Nanotechnol.*, 2016, **11**, 472.
4 S. Lim, D. Son, J. Kim, Y. B. Lee, J.-K. Song, S. Choi, D. J. Lee, J. H. Kim, M. Lee, T. Hyeon and D.-H. Kim, *Adv. Funct. Mater.*, 2015, **25**, 375.
5 M. Amjadi, A. Pichitpajongkit, S. Lee, S. Ryu and I. Park, *ACS Nano*, 2014, **8**, 5154.
6 S. Yang, Y. C. Chen, L. Nicolini, P. Pasupathy, J. Sacks, B. Su, R. Yang, D. Sanchez, Y. F. Chang, P. Wang, D. Schnyer, D. Neikirk and N. Lu, *Adv. Mater.*, 2015, **27**, 6423.
7 X. Wang, L. Dong, H. Zhang, R. Yu, C. Pan and Z. L. Wang, *Adv. Sci.*, 2015, **2**, 1500169.
8 C. M. Boutry, A. Nguyen, Q. O. Lawal, A. Chortos, S. Rondeau-Gagne and Z. Bao, *Adv. Mater.*, 2015, **27**, 6954.
9 S. Gong, W. Schwalb, Y. Wang, Y. Chen, Y. Tang, J. Si, B. Shirinzadeh and W. Cheng, *Nat. Commun.*, 2014, **5**, 3132.
10 E. Roh, B.-U. Hwang, D. Kim, B.-Y. Kim and N.-E. Lee, *ACS Nano*, 2015, **9**, 6252.
11 X. Li, R. Zhang, W. Yu, K. Wang, J. Wei, D. Wu, A. Cao, Z. Li, Y. Cheng, Q. Zheng, R. S. Ruoff and H. Zhu, *Sci. Rep.*, 2012, **2**, 870.
12 S. Choi, H. Lee, R. Ghaffari, T. Hyeon and D. H. Kim, *Adv. Mater.*, 2016, **28**, 4203.
13 S. Y. Hong, Y. H. Lee, H. Park, S. W. Jin, Y. R. Jeong, J. Yun, I. You, G. Zi and J. S. Ha, *Adv. Mater.*, 2016, **28**, 930.
14 J. Park, M. Kim, Y. Lee, H. S. Lee and H. Ko, *Sci. Adv.*, 2015, **1**, e1500661.
15 K. K. Kim, S. Hong, H. M. Cho, J. Lee, Y. D. Suh, J. Ham and S. H. Ko, *Nano Lett.*, 2015, **15**, 5240.
16 Z. Wang, S. Wang, J. Zeng, X. Ren, A. J. Chee, B. Y. Yiu, W. C. Chung, Y. Yang, A. C. Yu, R. C. Roberts, A. C. Tsang, K. W. Chow and P. K. Chan, *Small*, 2016, **12**, 3827.
17 Q. Sun, H. Kim do, S. S. Park, N. Y. Lee, Y. Zhang, J. H. Lee, K. Cho and J. H. Cho, *Adv. Mater.*, 2014, **26**, 4735.
18 T.-C. Li, C.-F. Han, K.-T. Chen and J.-F. Lin, *J. Disp. Technol.*, 2013, **9**, 577.
19 P. Gutruf, C. M. Shah, S. Walia, H. Nili, A. S. Zoolfakar, C. Karnutsch, K. Kalantar-zadeh, S. Sriram and M. Bhaskaran, *NPG Asia Mater.*, 2013, **5**, e62.
20 M. Ramuz, B. C. Tee, J. B. Tok and Z. Bao, *Adv. Mater.*, 2012, **24**, 3223.
21 X. Zhang, S. Hu, M. Wang, J. Yu, Q. Khan, J. Shang and L. Ba, *Nanotechnology*, 2015, **26**, 115501.
22 D. J. Lipomi, M. Vosgueritchian, B. C. Tee, S. L. Hellstrom, J. A. Lee, C. H. Fox and Z. Bao, *Nat. Nanotechnol.*, 2011, **6**, 788.
23 B. U. Hwang, J. H. Lee, T. Q. Trung, E. Roh, D. I. Kim, S. W. Kim and N. E. Lee, *ACS Nano*, 2015, **9**, 8801.
24 Y.-C. Lai, B.-W. Ye, C.-F. Lu, C.-T. Chen, M.-H. Jao, W.-F. Su, W.-Y. Hung, T.-Y. Lin and Y.-F. Chen, *Adv. Funct. Mater.*, 2016, **26**, 1286.

 This journal is © The Royal Society of Chemistry 2016

25 S.-H. Bae, Y. Lee, B. K. Sharma, H.-J. Lee, J.-H. Kim and J.-H. Ahn, *Carbon*, 2013, **51**, 236.
26 T. Q. Trung, S. Ramasundaram, B. U. Hwang and N. E. Lee, *Adv. Mater.*, 2016, **28**, 502.
27 Z. Liu, D. Qi, P. Guo, Y. Liu, B. Zhu, H. Yang, Y. Liu, B. Li, C. Zhang, J. Yu, B. Liedberg and X. Chen, *Adv. Mater.*, 2015, **27**, 6230.
28 J. Park, D. Tahk, C. Ahn, S. G. Im, S.-J. Choi, K.-Y. Suh and S. Jeon, *J. Mater. Chem.*, 2014, **2**, 2316.
29 B. J. Kim, D. H. Kim, Y.-Y. Lee, H.-W. Shin, G. S. Han, J. S. Hong, K. Mahmood, T. K. Ahn, Y.-C. Joo, K. S. Hong, N.-G. Park, S. Lee and H. S. Jung, *Energy Environ. Sci.*, 2015, **8**, 916.
30 H. Morikawa and M. Fujita, *Thin Solid Films*, 2000, **359**, 61.

Published on 05 October 2016. Downloaded by Incheon National University on 18/11/2016 05:18:55.